

Submitted for presentation at the “9th International Symposium on Special Topics in Chemical Propulsion (9-ISICP)”, 9-13 July, 2012, Quebec City, CANADA; and, for publication in the International Journal of Energetic Materials and Chemical Propulsion (IJEMCP).

DEFORMATION-INDUCED HOT SPOT CONSEQUENCES OF AP AND RDX CRYSTAL HARDNESS MEASUREMENTS

R.W. Armstrong*, S.G. Bardenhagen**, and W.L. Elban***

*University of Maryland, College Park, MD 20742, U.S.A.

**Wasatch Molecular, Inc., Salt Lake City, UT 84103, U.S.A.

***Loyola University Maryland, Baltimore, MD 21210, U.S.A.

ABSTRACT

Elastic, plastic, and cracking indentation measurements obtained in nano- to micro- to macro-indentation hardness tests of AP and RDX crystals are usefully described on a hardness stress – strain basis and are assessed in terms of the dislocation pile-up avalanche mechanism for hot spot generation associated with sudden crack formation. The model considerations lead to interpretation of a particle size influence on the drop-weight height for 50% probability of onset of reaction, now extended to include recently reported results for ϵ -HNIW crystals. These considerations are extended to deformation of individual or interacting groups of crystals when incorporated within a composite formulation and in relation to the potential brittleness of the binder material if undergoing transition to a glassy structure.

Keywords: AP, RDX, hardness, dislocation pile-up avalanches, hot spots, crystal size dependence, composite formulations, particle contiguity

Primary Technical Area: Insensitive Munitions
Secondary Technical Area: Hazard Reduction and Safety Aspects

1. INTRODUCTION

Ionically-bonded ammonium perchlorate (AP), $[\text{NH}_4.\text{ClO}_4]$, and molecularly-bonded cyclotrimethylenetrinitramine (RDX), $[\text{CH}_2.\text{N}.\text{NO}_2]_3$, crystals normally exhibit respective diamond pyramid micro-hardness values of, say, $\sim 100+$ MPa and ~ 230 MPa, in which the hardness indentations exhibit cracking. The micro-hardness values are increased to ~ 1.0 and ~ 2.0 GPa, respectively, in nano-indentation tests made, perhaps surprisingly, without initiations of cracking. Such crystals are incorporated within plastically-bonded composite formulations employing binders having ambient tensile strengths in the range of ~ 1.0 to ~ 10 MPa. The binder strengths can be increased by one or more orders of magnitude under high rate loading (or lowered temperature) and under increased pressure conditions associated with transformation to the glassy state. An important question for design of insensitive material properties in a mechanical environment and for safety concerns is how to prevent unintentional reaction of the materials. In the present report, the elastic, plastic, and cracking indentation hardness properties of such crystals are described in relation to the dimensional scale at which plastic deformation and cracking are observed to occur and especially are considered in relation to the size of generated hot spots. The analysis connects with the crystal size dependence for onset of reaction of loose piles of crystals when subjected to drop-weight impact testing. And relevance to crystal particle behaviors in energetic material formulations is of concern when an increase in binder strength occurs on transition to a brittle glassy state.

2. HARDNESS OF AP AND RDX CRYSTALS

With modern instrumentation available in conventional compression test systems applicable at macro- and micro-scales and with the very high resolution capabilities of load – displacement measurements built into nano-indentation hardness testing equipment, the complete elastic, plastic, and cracking behaviors of crystal/polycrystal/polyphase materials are able to be monitored quantitatively (Armstrong and Elban, 2012). Such load – displacement measurements are able to be transformed, for comparison of different hardness test results, into effective stress – strain curves based on a continuous ball indentation test. Because of the very sensitive load/displacement measurement capabilities available in most nanoindentation test systems such deformation begins with an initial load - displacement behavior that follows the predicted elastic Hertzian dependence for contact of the spherically-capped indenter tip.

2.1. Nano- to Micro- to Macro-Hardness of AP Crystals

Figure 1 shows the fit of such (dashed) elastic loading prediction to initial load – displacement measurements for an AP $\{210\}$ crystal surface reported by Lucca et al (2006). The Hertzian equation for the initial loading dependence is

$$P = (8D/9)^{1/2} E_r h_e^{3/2} \quad (1)$$

In Eq. (1), D is the effective ball diameter, h_e is the elastic penetration depth, and $E_r = \{[(1-\nu_S^2)/E_S] + [(1-\nu_B^2)/E_B]\}^{-1}$ for the effective elastic modulus of the crystal. In Eq. (1), ν_S , E_S and ν_B , E_B are the Poisson's ratio and Young's modulus for specimen and ball, respectively. For the dashed elastic curve prediction in Fig. 1, $\nu_S \sim 0.3$ and $E_S = 20.5$ GPa for AP and $\nu_B = 0.068$ and $E_B = 1145$ GPa for the diamond indenter tip. In this case, the value of $D = 579$ nm was determined by fit of Eq. (1) to the highest elastic deformation point shown at the (b1) coordinates 5.0 nm, 5.2 μ N; a larger $D = 940$ nm had been employed previously by Armstrong and Elban (2012) for an average fit to the total elastic deformation behavior. Determination of the value of D importantly relates to reliably determining E_r as also can be evaluated from the unloading behavior by means of a modified Hertzian analysis that is indicated for the generally steeper plastic unloading dependence (Lucca et al, 2006). In Fig. 1, the marked (b1) – (b4) “pop-in” deformations at increasing load values signal the onset of local bursts of plastic deformation. Cracking was not reported for this particular test result.

The hardness stress-strain dependence derived from the deformation curve of Fig. 1 and from reported additional higher load test results is shown in Fig. 2. Other (filled triangle) diamond pyramid micro-hardness measurements and additional (open square) macroscopically-determined continuous loading stress – strain results obtained with a hardened steel ball are shown. For this figure, the hardness stress is obtained from the load, P , divided by the projected contact area, $\pi d^2/4$, in which d is the (surface) contact diameter, and the hardness strain is conveniently expressed as d/D , in which D is the effective ball diameter. The elastic deformation is contained within the (d/D) measurement, even for plastic indentations, and the elastic hardness stress, σ_H , follows the Hertzian expression

$$\sigma_H = (4/3\pi)E_r(d_e/D) = (4/3\pi)E_r(2h_e/D)^{1/2} \quad (2)$$

In Eq. (2), d_e is the counterpart elastic contact diameter corresponding to h_e in the Hertzian equation. Conversion factors for ball-type (d/D) values are known for different polygonally-shaped micro-indentations. For a diamond pyramid impression, the hardness strain, (d/D) , has a value of 0.375.

The four pairs of (filled-to-open) circle points in Fig. 2 connect the before-and-after b-level “pop-in” stresses whereas the inverted open triangle points were reported by Lucca et al. as individually determined micro-hardness values. There was an absence of cracking for penetration depths > 140 nm, that is, $\gg 50$ nm that determined the extent of indenter penetration for the test result in Fig. 1. Cracking was associated with all of the separately determined (Elban and

Armstrong, 1998) closed-triangle diamond pyramid measurements shown at $(d/D) = 0.375$ in Fig. 2. And Fig. 3 shows one such (00-1) crack produced at an aligned diamond pyramid micro-indentation put into a similarly identified $\{210\}$ crystal surface. As indicated in the Fig. 2 caption, the crack was produced by a sessile-type dislocation reaction at intersecting dislocation pile-ups spread over micro-scale dimensions in juxtaposed slip traces that are just discernable in the micrograph. The larger extent of the top-side portion of the residual indentation provides evidence that crack growth has facilitated subsequent further breakout of the plastic deformation. Lastly, at the lowest (open square) stress level for the continuous macro-indentation test result shown in Fig. 2, a very prominent crack was initiated at the discontinuous stress drop shown at $(d/D) \sim 0.8$. This indicates that stress build-up occurs locally at the slip band level until sudden release of dislocations occurs through the crack surfaces in an avalanche of deformation.

2.2. Nano- and Micro-Hardness Measurements on RDX

Plastic deformation on anisotropic slip systems is more extremely localized in RDX than for AP (Armstrong and Elban, 2004). Figure 4 shows a comparison of diamond point nano- and 1.5875 mm steel ball-type micro-hardness test results obtained in separate studies made on several RDX crystals. Also, comparison is shown with a macroscopic (6.35 mm) steel ball result obtained on an NaCl crystal based on the same effective stress – strain description. The filled circle points on the NaCl and RDX curves are converted diamond pyramid hardness measurements made on these same crystals. Thus, the ordinate hardness stress, σ_H , is either the mean pressure on an actual spherical ball indenter or on a diamond nano-indenter tip or is the actual diamond pyramid hardness measurement. The open circle points along the Hertzian lines or at the end points are elastic cracking stresses predicted for the different respective D values that are provided (Armstrong and Elban, 2012). The elastic, plastic and cracking behaviors span test results reported at nano-, micro-, and macro-indentation hardness scales.

The relatively small range in hardness stress levels between the open square micro-indentation measurements shown for RDX, including the onset of dislocation-induced cracking, and the open circle elastic cracking stress predicted at the same ball size, when compared to the same type larger spread in stress levels shown for NaCl in Figure 4, gives indication of the relative brittleness of RDX and defines the narrow range in stress that is available for influence of loading rate on increasing the plastic resistance to flow. The higher open triangle points for RDX crystal hardness values determined with a D value of 2.96 microns in nano-indentation tests, without cracking, were measured for different crystal surface conditions (Ramos et al., 2011). In this case, the much smaller size of the RDX nano-indentations and corresponding small plastic deformation zones were insufficient to produce cracking by dislocation reaction/coalescence or to grow invisible small cracks to visible size, in contrast to the lower stress case of

micrometer-scale ball-type hardness indentations (open square) put into another RDX crystal surface.

3. DISLOCATION PILE-UP INDUCED CRACKING AND HOT SPOTS

The different RDX indentation sizes in Fig. 4 may be compared to estimations of hot spot sizes required for RDX initiation on the basis of thermal energy conversion. Walley et al, (2006) have tabulated estimations for RDX (also known as cyclonite) in the range of 0.01 to 10 μm , with associated need of critical temperatures, respectively, of 820 to 385 K. Thus, a reasonable estimated hot spot size of, say, 1.0 μm and 485 K temperature rise could be associated with breakthrough of a dislocation pile-up spread over a slip length of 10 to 100 μm . This does not preclude limited chemical decompositions being initiated by the smallest imaginable probing contact of nano-indentations or with atomic force indentations, as described recently for important atomic scale observations made on trinitrophenol (TNP) crystals by Kovalev and Sturm (2011).

Micrometer-scale cracking measurements for both AP and RDX crystals have been employed also to determine the effective surface energy for cracking based on a log/log dependence of applied load on crack size via an indentation fracture mechanics analysis (Armstrong and Elban, 2012). Very importantly, the determined fracture surface energy for RDX was found to be $\sim 2\text{X}$ larger than the thermodynamic value. The relatively low energy result is interpreted to mean that *hot spots are unlikely to be associated with the growth of cracks!* Rather, the mechanism of hot spot development is attributed to a plastic deformation mechanism of crack initiation with sudden accompanying dissipation of the stored energy in the dislocation pile-up. And the absence of cracking at nano-scale dimensions for both AP and RDX crystals appears to be equally significant in demonstrating *needed plasticity-associated micrometer-scale dimensions for generation of hot spots leading to explosive decompositions.*

On the basis of this plastically induced hot spot model description, dislocation pile-ups are proposed to be held up at mutually-intersecting slip bands or at other type obstacles within the crystals and/or, especially, between crystals at their boundaries until sufficient stress concentration is reached to produce discontinuous cracking and the stored energy within the pile-ups is suddenly dissipated as heat. The contiguity aspect of particle-to-particle contacts in the drop-weight impact tests is thought to be a prime consideration for hot spot initiations. Such hot spots are a consequence therefore of the rapid transformation of local plastic work into heat during the avalanching mechanism of dislocations exiting the free crack surfaces (Armstrong, 2009).

4. CRYSTAL SIZE DEPENDENCE OF INITIATION

The dislocation pile-up avalanche description leads to prediction of greater hot spot heating for larger dislocation pile-ups taken to be proportional in length to the crystal size, ℓ . The model description has been expressed most recently in the implicit equation applied to prediction for loose piles of crystals of a log/log dependence for the drop-weight height for 50% probability of onset of reaction, H_{50} , and the reciprocal square root of crystal size, ℓ , in the relationship (Armstrong and Elban, 2010).

$$\log H_{50} \propto \left(\frac{nkT}{W_0} \right) \log \left(f \{ \Delta T, T, \dots \} \ell^{-1/2} \right) \quad (3)$$

In Eq. (3), n is a number for the exponential dependence of stress on drop-height, k is Boltzmann's constant, T is temperature, W_0 is an energy coefficient for the dislocation activation volume dependence on shear stress, and ΔT is the temperature rise needed for initiation.

A log/log dependence of H_{50} on $\ell^{-1/2}$ had previously been established for two types of RDX crystals and for one set of measurements made on CL-12 material. Figure 5 shows addition of drop-weight impact results reported recently by (Elbeih et al, 2011) for ϵ -HNIW (CL-20) crystals of different sizes. The similar trend shown for the new results is encouraging. The smallest particle size material exhibits impact sensitivity comparable to that shown to be predicted for RDX NWC material. Elbeih et al. give emphasis to the importance of crystal perfection and purity. Previously, the vertical spread shown for three closed circle points of RDX NAVSWC material at $\ell = 0.25$ mm particle size had been attributed to variation in the crystal perfection.

5. CRYSTAL – BINDER CONCERNS FOR INITIATION

Current research is directed to extending such understanding of individual energetic crystal properties to their behaviors in composite material formulations and to do so by investigating both model inert material systems such as polymer-bonded sucrose (PBS) materials (Bardenhagen et al., 2011) or by investigating individual aspects of actual material compositions, such as crystal-binder interfacial adhesions (Yeager et al., 2012). Comparable nano-indentation test results to those of AP and RDX have been reported for sucrose by Ramos and Bahr (2007).

Figure 6 shows a series of specimen PBS volumes clipped to smaller rectangular dimensions in an effort to determine the size scale at which a representative volume element (rve) may be achieved, hopefully, at a limiting smallest dimensional scale. Particle size strengthening effects persist in such composite

materials (Siviour et al, 2004) with indication of strength dependence on the reciprocal square root of crystal particle size. Here, characterizations of features such as average crystal dimensions, distribution of sizes, crystal-polymer bonding, porosity, and such stereological concerns as the material contiguity parameter, C , for particle-to-particle contacts are of interest. With regard to Fig. 6, formulated sample material morphologies are being obtained by x-ray tomography and an image analysis program (Ketcham, 2005) is being employed to characterize distributions of geometric features including grain and void sizes, and contact area and number density (Bardenhagen et al., to appear). These properties are expected to correlate with hardness (as determined for C below) and sensitivity (in the case of energetic formulations, where C is likely related to hot spot density as previously mentioned in Section 3). Damaged material is being characterized also to determine associated changes in morphology and (ultimately) sensitivity implications.

As mentioned in the **INTRODUCTION**, a normal binder material might desirably exhibit a low, near liquid-like, strength level and have associated extensive flow properties. In the first instance, such combination of properties contributes to ease of composite fabrication even with infiltration at high packing density of the crystals and also would desirably lower operating stress levels needed in manufactured product shapes as well as lessen damage effects from external mechanical stimuli. However, at increasing loading rate and pressure, there is concern for a rather sudden increase in mechanical strength and embrittlement of the binder material accompanying its transition to the glassy state (Bohn, 2012). Strength levels on the order of 100 MPa or greater are achievable. Thus, these strength levels reach into the range of individual crystal strengths and could cause transition to a more concrete-like composite structure. Brittle cracking of the binder phase would involve sudden release of pent-up dislocation pile-up deformations within the crystal constituents and be associated as well with rapid load transfer to the crystals, undoubtedly with enhanced effect at nearby local particle-to-particle contacts.

These same types of considerations are analogously demonstrated to apply for hardness property measurements made on the important industrial WC-Co cermet materials (Armstrong, 2011). The contiguity, C , of WC particles has been shown to enter into the composite micro-hardness measurement, H , in accordance with the relationship

$$H = H_{WC}V_{WC}C + H_m(1 - V_{WC}C) \quad (4)$$

In Eq. (4), H_{WC} is the micro-hardness of the WC constituent that, again, follows a reciprocal square root of size dependence, V_{WC} is the volume fraction, and H_m is the hardness of the Co binder constituent that also follows a reciprocal square root of mean free path dependence for its hardness level. The weaker Co phase is

known to be a main determinant of the composite material properties, as is coming to be better known to apply for the binder phase in energetic material formulations.

Consequently for energetic material formulations, there is emphasis on the viscoplastic properties of the binder material and its potential transition to the glassy phase, especially under condition of increased pressure (Knauss and Sundaram, 2004). A constitutive equation description for such polymeric materials has been given by Zerilli and Armstrong (2007) with application to polymethylmethacrylate (PMMA -- Plexiglass) and to polytetrafluoroethylene (PTFE -- Teflon). Rittel and Brill (2008) have investigated the static and dynamic deformation properties of PMMA with special regard for the embrittlement effect of material confinement and induced shear banding behavior. The association of dislocation pile-up avalanches with adiabatic shear banding (ASB) behavior has been reviewed for counterpart metal and alloy material deformation behaviors at high strain rates by Armstrong and Walley (2008). Alternatively, Wiegand and Reddingius (2005) have pointed to the effect of confinement pressure applied to explosives on preventing cracking and enhancing plastic flow, presumably below the shifted glass transition temperature of the binder. Further research is needed to sort out the effects. Current research involves extending the above-mentioned Z-A equations into the glass transition region and incorporating the effect of strain rate and pressure on unwanted glass formation.

6. SUMMARY

Hardness measurements of AP and RDX crystal properties over a range in scale from nano- to micro- to macro-measurements show a special relationship of elastic loading followed by plastic deformation and, in turn, the sudden generation of cracking. The resultant indentation behaviors support a proposed mechanism for hot spot generation in which a dislocation pile-up avalanche is suddenly released from a blocking obstacle and passes through newly generated crack surfaces. An accompanying prediction of crystal size dependence for such hot spot generation and onset of reaction of RDX and CL-12 crystals in drop-weight impact sensitivity tests is added to with display of recent measurements reported for ϵ -HNIW crystals. Application of these considerations to more complicated crystal/binder interactions within composite energetic material formulations is addressed, particularly, relating to concern for glassy embrittlement of the polymer binder phase and consequent promotion of hot spots through suddenly induced cracking of the binder phase and release of similarly developed pent-up internal dislocation pile-up strains from within the encapsulated energetic crystals.

7. REFERENCES

Armstrong, R.W., (2009) Dislocation Mechanics Aspects of Energetic Material Composites, *Rev. Adv. Mater. Sci.*, 19, pp. 13-40.

Armstrong, R.W., (2011) The Hardness and Strength Properties of WC-Co Composites, *Materials*, 4(7), pp. 1287-1308.

Armstrong, R.W, and Elban, W.L., (2004) Dislocations in Energetic Crystals, In F.R.N. Nabarro and J.P. Hirth, Eds., *Dislocations in Solids*, Oxford, U.K.: Elsevier B.V., Vol. 12, Chap. 69, pp. 403-446.

Armstrong, R.W. and Elban, W.L., (2010) From Intermolecular Shearing to Composite Behavioral Predictions for Initiation of Energetic Materials, *Proc. 14th Intern. Detonation Symp.*, Office of Naval Research Report ONR-351-10-185, pp. 1430-1439.

Armstrong, R.W. and Elban, W.L., (2012) Hardness Properties across Multiscales of Applied Loads and Material Structures, *Mater. Sci. Tech.*, 12 pp., in print.

Armstrong, R.W. and Walley, S.M. (2008) High Strain Rate Properties of Metals and Alloys, *Int. Mater. Rev.*, 53(3), pp. 105-128.

Bardenhagen, S.G., et al., (2012) Detailed Characterization of PBX Morphology for Mesoscale Simulations, *Shock Compression of Condensed Matter – 2011*, AIP Conf. Proc. 1426, pp. 637-640.

Bardenhagen, S.G., et al., (to appear) Mesoscale Investigations into the Role of Structure on PBX Sensitivity, *JANNAF 37th Propellant and Explosives Development and Characterization Meeting*, JANNAF Conf. Proc.

Bohn, M.A., (2012) Impacts on the Loss Factor Curve and Quantification of Molecular Rearrangement Regions from it in Elastomer Bonded Energetic Formulations, In R.W. Armstrong et al., Eds., *Energetics Science and Technology in Central Europe*, College Park, MD: CALCE EPSC Press, Chap. 10, pp. 195-235.

Elbeih, A., et al., (2011) Path to ϵ -HNIW with Reduced Impact Sensitivity, *Cent. Eur. J. Energ. Mater.*, 8(3), pp. 173-182.

Ketcham, R.A., (2005) Computational Methods for Quantitative Analysis of Three-Dimensional Features in Geological Specimens, *Geosphere*, 1(1), pp. 32-41.

Knauss, W.G. and Sundaram, S., (2008) Pressure-sensitive Dissipation in Elastomers and Its Implications for the Detonation of Plastic Explosives, *J. Appl. Phys.*, 96(12), pp. 7254-7261.

Kovalev, A. and Sturm, H., (2011) Observation of Nanoscale Hot-Spot Generation on a 2,4,6-trinitrophenol (TNP) Single Crystal, *Surf. Sci.*, 605, pp. 1747-1753.

Lucca, D.A., et al., (2006) Investigation of Ammonium Perchlorate by Nanoindentation, *Mater. Sci. Tech.*, 22(4), pp. 396-401.

Ramos, K.J. and Bahr, D.F., (2007) Mechanical Behavior Assessment of Sucrose Using Nanoindentation, *J. Mater. Res.*, 22(7), pp. 2037-2045

Ramos, K.J. et al., (2011) Defect and Surface Asperity Dependent Yield during Contact Loading of an Organic Molecular Crystal, *Philos. Mag.*, 91, pp. 1276-1285.

Rittel, D. and Brill, A. (2008) Dynamic Flow and Failure of Confined Polymethylmethacrylate, *J. Mech. Phys. Sol.*, 56, pp. 1401-1416.

Siviour, C.R., et al., (2004) Particle Size Effects on the Mechanical Properties of a Polymer Bonded Explosive, *J. Mater. Sci.*, 39(4), pp. 1255-1258.

Walley, S.M. et al., (2006) Crystal Sensitivities of Energetic Materials, *Mater. Sci. Tech.*, 22(4), pp. 402-413.

Wiegand, D.A. and Reddingius, B., (2005) Mechanical Properties of Confined Explosives, *Energ. Mater.*, 23, 75-98.

Yeager, J., et al., (2012) Nanoindentation of Molecular Composites to Simulate Deformation and Failure, *Mater. Sci. Tech.*, 10 pp., in print.

Zerilli, F.J. and Armstrong, R.W., (2007) A Constitutive Equation for the Dynamic Deformation Behavior of Polymers, *J. Mater. Sci.*, 42(12), pp. 4562-4574.

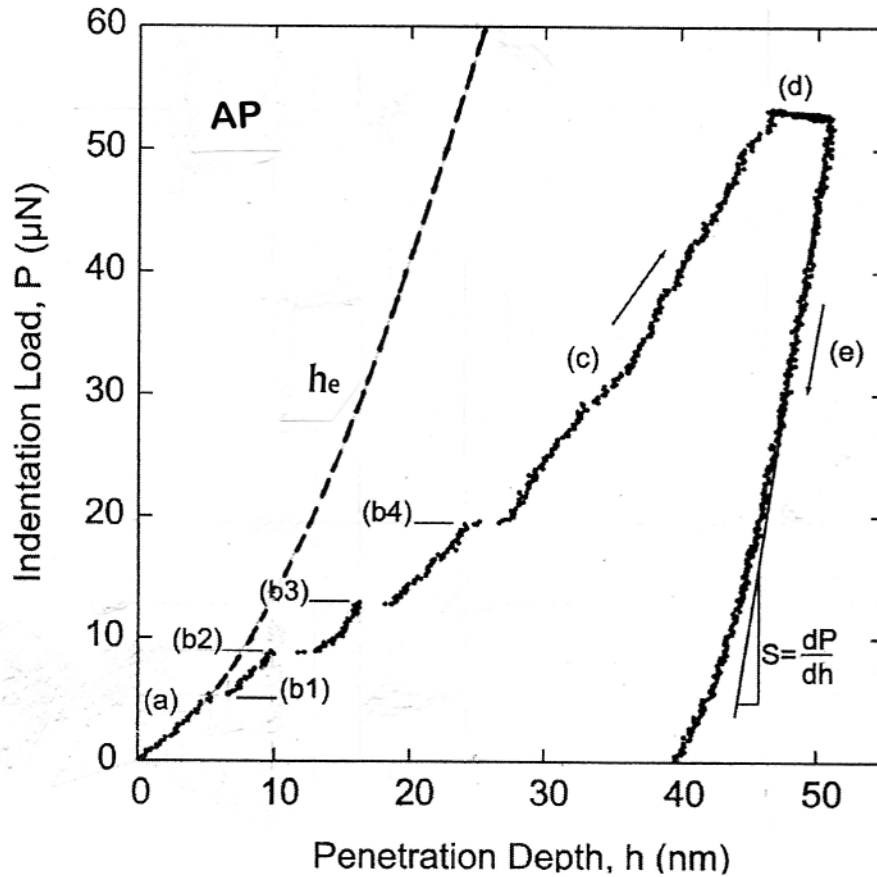


Figure 1. Nanoindentation test result for (210) AP crystal surface adapted to show the Hertzian elastic loading behavior based on the diamond indenter having a spherical tip with diameter, $D = 579$ nm, fitted to the penetration depth at the first pop-in, (b1), corresponding to $h = 5.0$ nm under load, P , of 5.2 μN ; see D.A. Lucca, M.J. Klopstein, O.R. Mejia, L. Rossetini and L.T. DeLuca, Mater. Sci. Tech., 22, [4], 396-401 (2006).

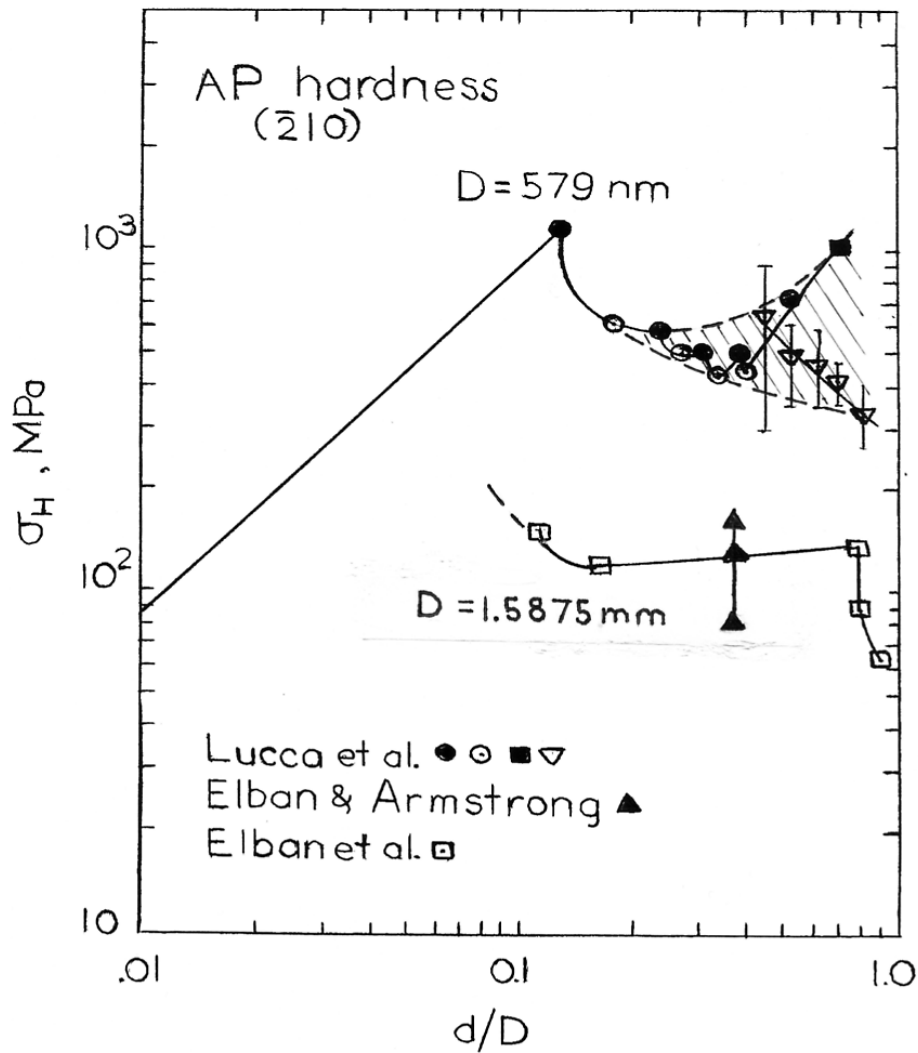


Figure 2. Hardness stress – strain dependencies for AP crystals from nano- to micro- to macro-test results: D.A. Lucca, M.J. Klopstein, O.R. Mejia, L. Rossetini, and L.T. DeLuca, *Mater. Sci. Tech.*, **22**, [4], 396-401 (2006); W.L. Elban and R.W. Armstrong, *Acta Mater.*, **46**, 6041-6052 (1998), [filled-triangle micro-hardness points]; W.L. Elban, P.J. Coyne, Jr., and R.W. Armstrong, “Mechanical Property Determination of Single Crystal Ammonium Perchlorate”, 1998, unpublished.

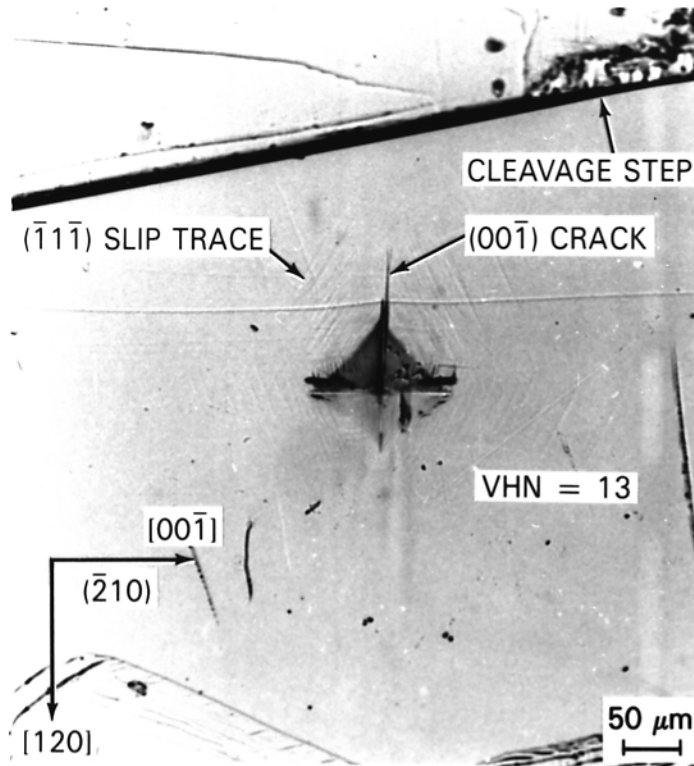


Figure 3. Aligned diamond pyramid indentation put into (-210) AP crystal surface, demonstrating greater plastic deformation in the vertical top direction associated with $(00-1)$ cracking produced at the intersection of $(-11-1)$ $[-101]$ and $(-111)[-10-1]$ slip systems to generate by dislocation reaction a crack-forming $[00-1]$ Burgers vector dislocation; after W.L. Elban and R.W. Armstrong, *Acta Mater.* **46**, 6041-6052 (1998).

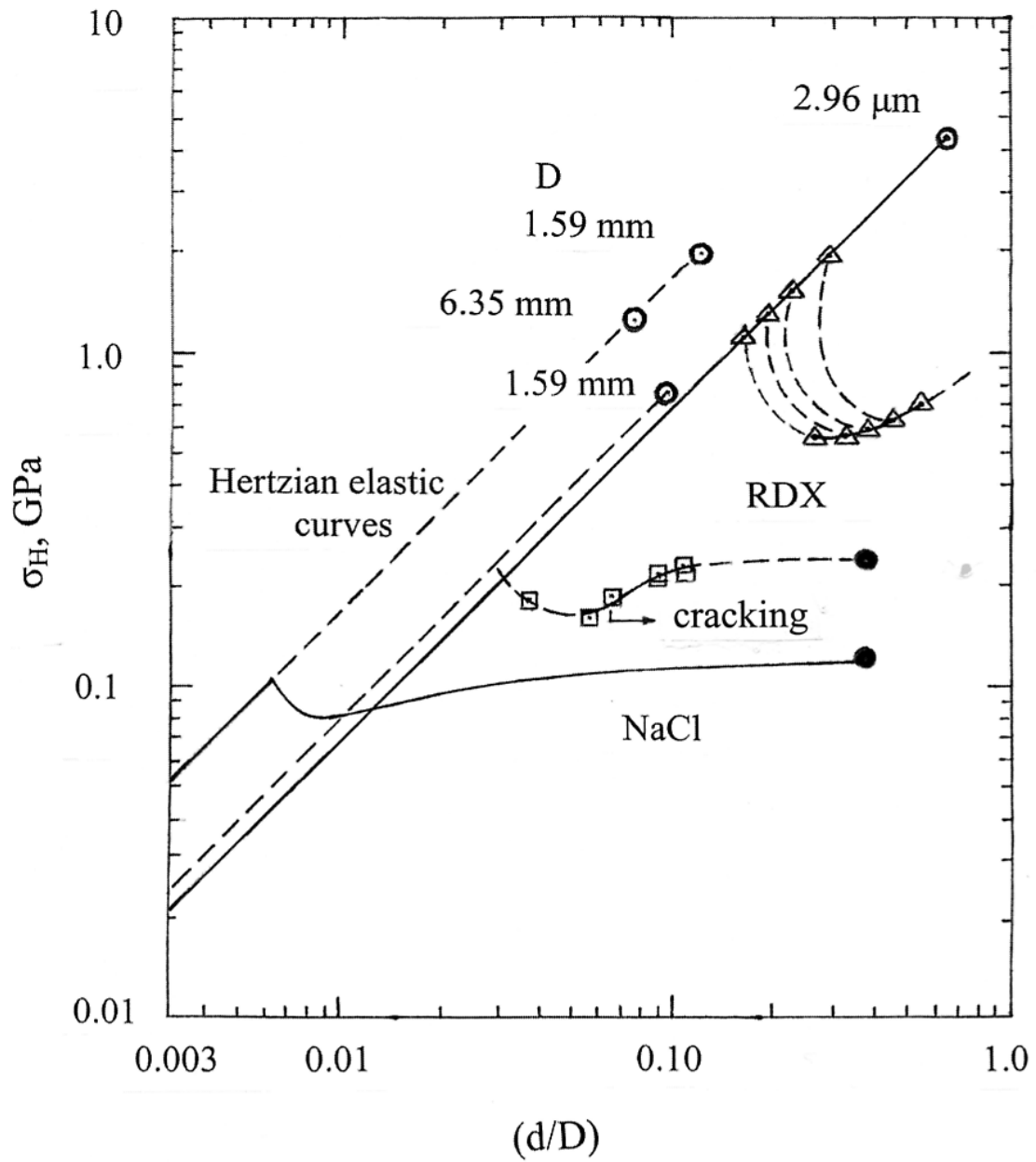


Figure 4. Nano-, micro-, and macro-indentation hardness stress – strain dependencies measured for RDX crystals in comparison with NaCl crystal results, as adapted from: R.W. Armstrong and W.L. Elban, *Mater. Sci. Tech.*, (2012) in print (2012); and K.J. Ramos, D.F. Bahr and D.E. Hooks, *Philos. Mag.*, **91**, [7-9], 1276-1285 (2011).

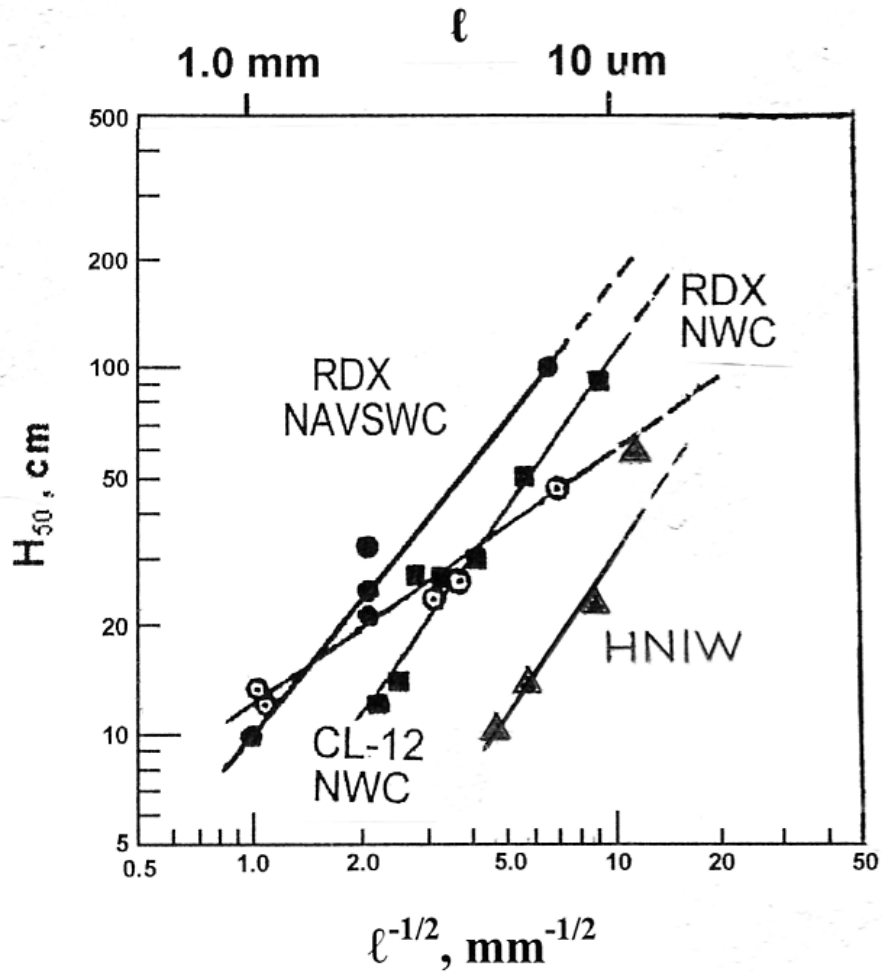


Figure 5. Drop-weight height, H_{50} , for 50% probability of initiation vs. inverse square root of crystal particle size, $\ell^{-1/2}$, for RDX, CL-12, and ϵ -HNIW (CL-20), s adapted from results reported by: R.W. Armstrong and W.L. Elban, Proc. 14th Intern. Deton. Symp., Office of Naval Research Report ONR-351-10-185, (2010); and, A. Elbeih, A. Husarova and S. Zeman, Cent. Eur. J. Energ. Mater., **8**, [3], 173-182 (2011).

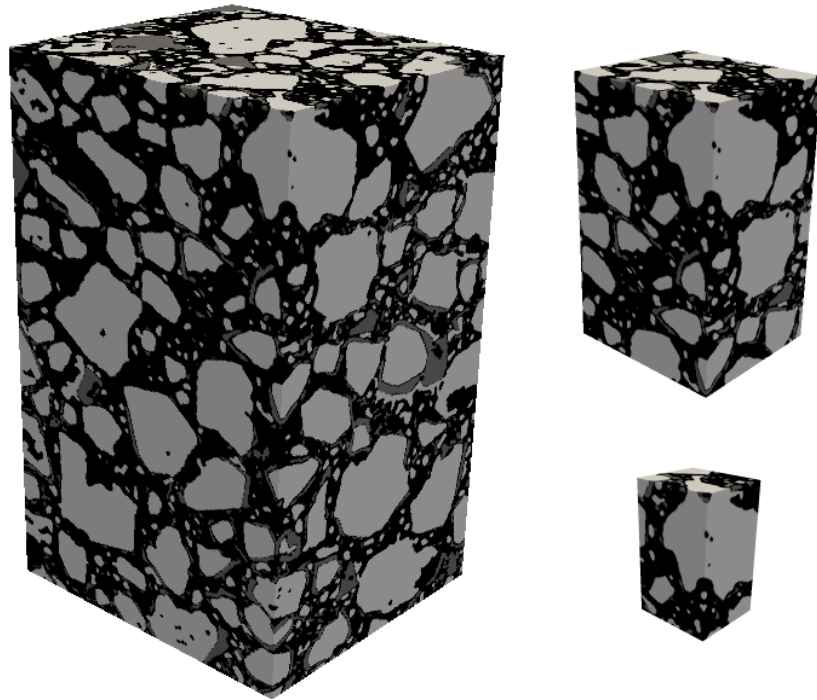


Figure 6. Composite polymer bonded sucrose (PBS) sections determined via tomography then for stereological characterization via Blob3D program for particle sizes, distribution, and particle-to-particle contacts (contiguities) in relation to establishing a representative volume element (RVE); S.G. Bardenhagen, H. Luo, R.W. Armstrong, and H. Lu, Shock Compression of Condensed Matter – 2011, AIP Conf. Proc. 1426, 637-640 (2012).